Science Advances
AAAS

advances.sciencemag.org/cgi/content/full/6/28/eabb7369/DC1

Supplementary Materials for

Dynamic metal-polymer interaction for the design of chemoselective and long-lived hydrogenation catalysts

Songhyun Lee, Seung-Jae Shin, Hoyong Baek, Yeonwoo Choi, Kyunglim Hyun, Myungeun Seo, Kyunam Kim, Dong-Yeun Koh, Hyungjun Kim*, Minkee Choi*

*Corresponding author. Email: linus16@kaist.ac.kr (H.K.); mkchoi@kaist.ac.kr (M.C.)

Published 8 July 2020, *Sci. Adv.* **6**, eabb7369 (2020)
DOI: 10.1126/sciadv.abb7369

This PDF file includes:

Figs. S1 to S13
Table S1
References

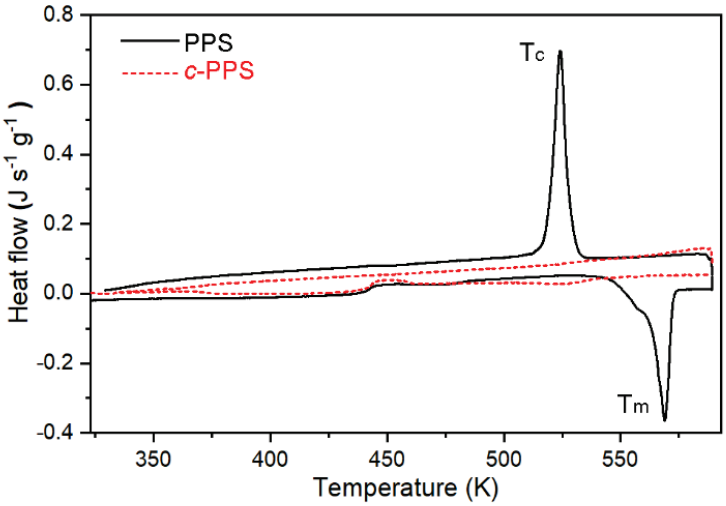

Fig. S1. Differential scanning calorimetry thermograms of PPS and *c*-PPS. The pristine PPS shows clear melting and crystallization behaviors at 569 K and 524 K, respectively, whereas *c*-PPS does not.

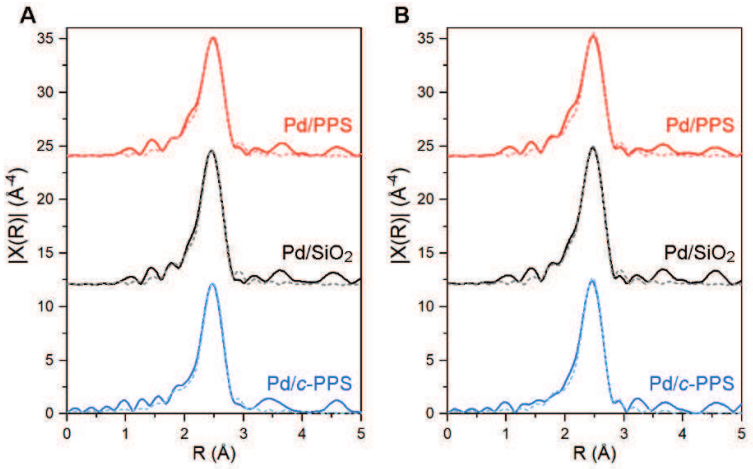

Fig. S2. Fourier transforms of k^3-weighted Pd K-edge EXAFS of the catalysts. (**A** and **B**) Pd catalysts before (A) and after (B) 200 h acetylene hydrogenation in an ethylene-rich stream. Solid line: experimental data, dashed line: fitted data.

A

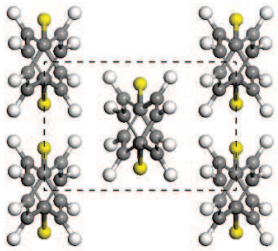

B

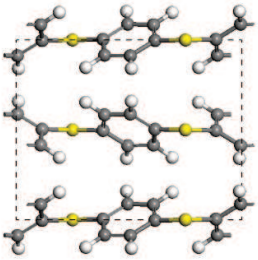

C

	Lattice parameter		
	X	Y	Z
Exp (Å)	8.670	5.610	10.260
DFT (Å)	8.271	5.548	10.376
RMSE (%)	4.604	1.104	1.132
FF (Å)	8.519	5.578	10.506
RMSE (%)	1.742	0.566	2.399

D

	Chain interaction energy
DFT (kcal/mol)	-50.824
FF (kcal/mol)	-50.597

Fig. S3. Models of PPS for simulation. (**A** and **B**) The front view (A) and the side view (B) of the PPS monomeric unit cell. (**C**) Lattice parameters for PPS monomeric unit cell. Experimental values were obtained from a previous study (*38*). Force field was abbreviated as "FF". (**D**) Chain interaction energies calculated by DFT and FF. They were calculated by the difference between the monomeric unit cell energy and twice the energy of a single chain.

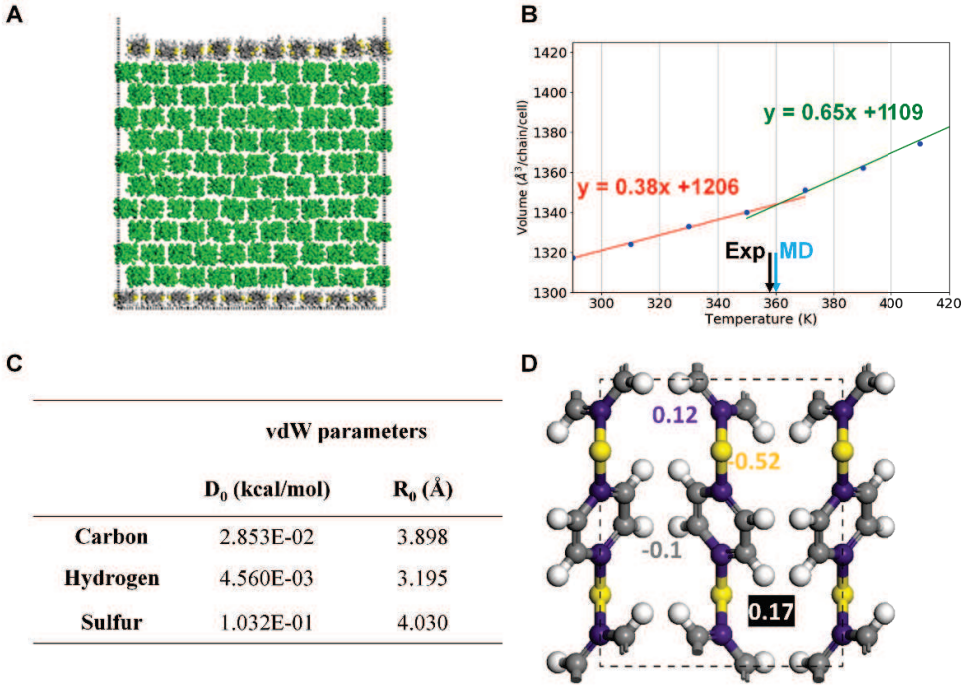

	vdW parameters	
	D_0 (kcal/mol)	R_0 (Å)
Carbon	2.853E-02	3.898
Hydrogen	4.560E-03	3.195
Sulfur	1.032E-01	4.030

Fig. S4. Force field values for MD simulation. (**A**) The volume of a single polymer chain was calculated using Voronoi tessellation during MD simulation in the green region (*39*). (**B**) Averaged volume of the PPS chain as a function of temperature. The glass transition temperature calculated by MD is indicated using a light blue arrow (359 K); a black arrow indicates an experimental value (358 K). (**C**) vdW parameters for PPS chains. (**D**) Point charges for PPS chains. Carbon is shown in grey and purple. By symmetry, their charges are different: -0.1 and 0.12, respectively. Sulfur and hydrogen are shown in yellow and white with -0.52 and 0.17 as point charges, respectively.

A

	vdW parameters	
	D_0 (kcal/mol)	R_0 (Å)
Pd – C	3.701E-02	3.362
Pd – H	1.479E-02	3.043
Pd – S	3.100E+00	3.700

B

	Binding energy
DFT (kcal/mol)	-22.452
FF (kcal/mol)	-22.788

C

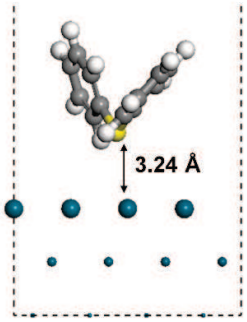

D

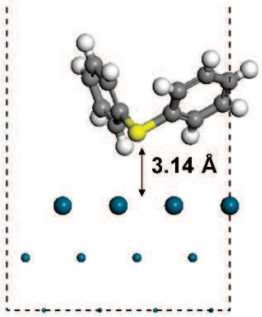

Fig. S5. vdW force field parameters between Pd and PPS. (**A**) Pairwise vdW parameters between Pd and atoms of PPS. (**B**) Binding energy of diphenyl sulfide on Pd (111). This energy is defined as $E_{bind} = E_{total} - E_{Pd\ (111)} - E_{diphenyl\ sulfide}$. (**C**) Optimized geometry of diphenyl sulfide on Pd (111) calculated using DFT. (**D**) Optimized geometry based on force field values. Distance between the top layer of Pd (111) surface and sulfur atom of molecule is figured out.

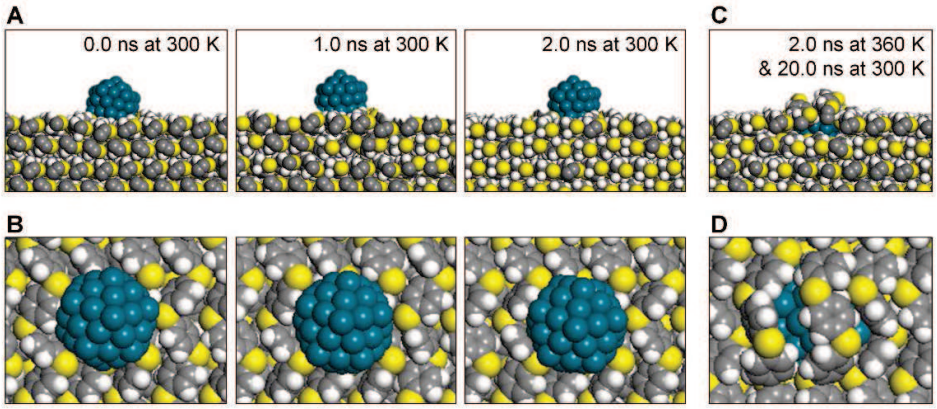

Fig. S6. MD snapshots of Pd particles supported on PPS surface. (**A** and **B**) The side view (A) and the top view (B) of the dynamics at 300 K. (**C** and **D**) The side view (C) and the top view (D) of the dynamics at 300 K after treating the system at 360 K for 2.0 ns. Pd, C, H, and S atoms are shown in dark cyan, grey, white, and yellow, respectively.

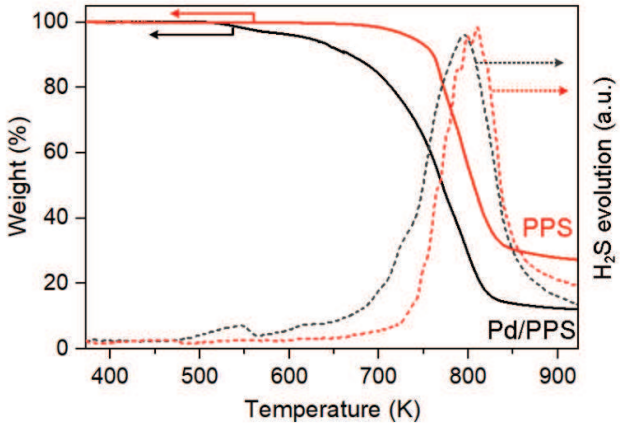

Fig. S7. Thermochemical stabilities of PPS and Pd/PPS. Weight loss and H_2S evolution of PPS (red) and Pd/PPS (black) during a temperature ramp (10 K min^{-1}) under H_2 atmosphere. Solid lines indicate weight loss detected by TGA and dotted lines indicate H_2S evolution detected by online quadrupole mass spectrometer (m/z = 34).

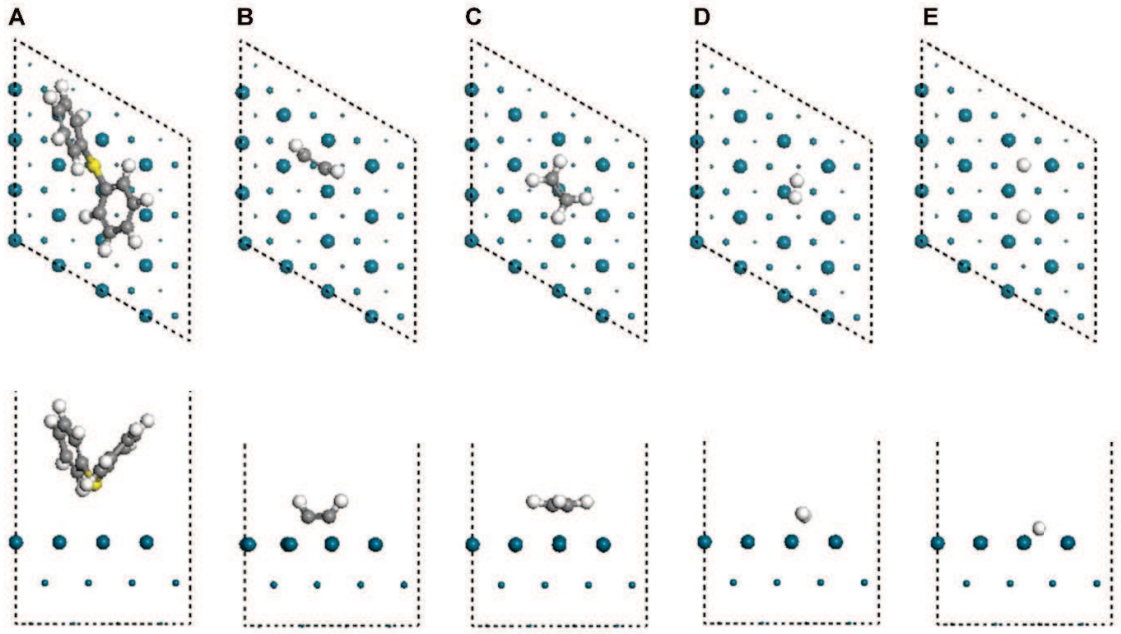

Fig. S8. DFT models to study the adsorption thermodynamics. (**A**) Diphenyl sulfide. (**B**) Acetylene. (**C**) Ethylene. (**D**) Associative hydrogen. (**E**) Dissociative hydrogen. The size of atoms in Pd (111) surface with three layers are shown differently, depending on the relative position of layers.

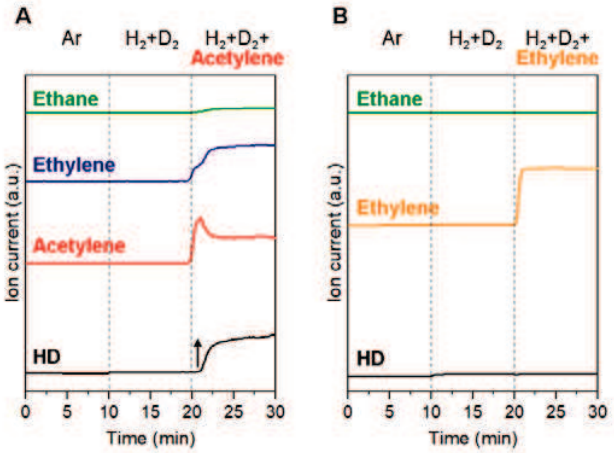

Fig. S9. Adsorption behaviors of H_2, acetylene, and ethylene on diphenyl sulfide-modified Pd/SiO_2. (**A**) H_2-D_2 isotope exchange at 373 K with and without co-injection of acetylene. (**B**) H_2-D_2 isotope exchange at 373 K with and without co-injection of ethylene.

A

	vdW parameters	
	D_0 (kcal/mol)	R_0 (Å)
Pd – C	10.0	2.10
Pd – H	1.479E-02	3.043

B

	Binding energy
DFT (kcal/mol)	-57.229
FF (kcal/mol)	-57.929

C

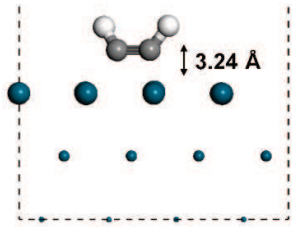

D

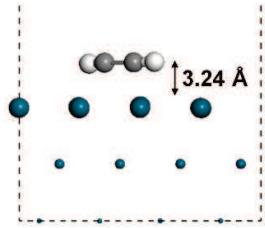

Fig. S10. vdW force field parameters between Pd and C_2H_2. (**A**) Pairwise vdW parameters between Pd and the atoms of C_2H_2. (**B**) Binding energy of acetylene on Pd (111). This energy is defined as $E_{bind} = E_{total} - E_{Pd\ (111)} - E_{acetylene}$. (**C**) Optimized geometry of acetylene on Pd (111) calculated by DFT. (**D**) Optimized geometry based on force field values. Distance between the top layer of Pd (111) surface and carbon atom of molecule is figured out.

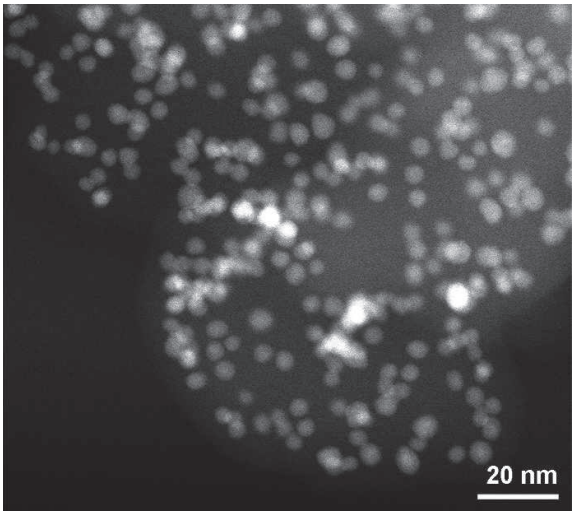

Fig. S11. HAADF-STEM image of Pd/PPS after 200 h acetylene hydrogenation in an ethylene-rich stream.

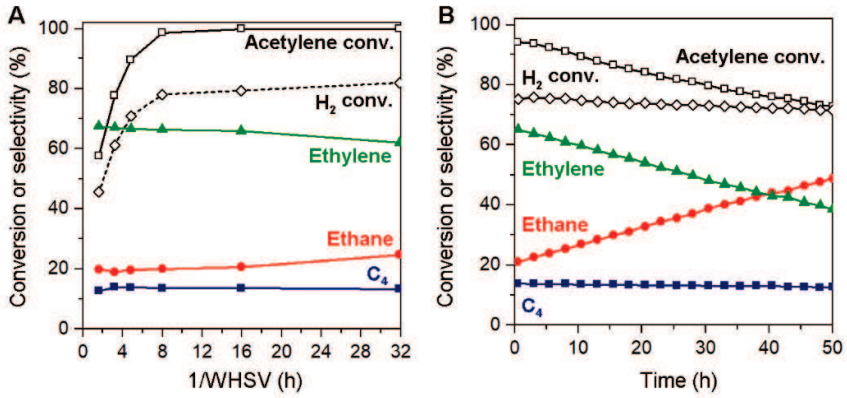

Fig. S12. Acetylene hydrogenation in an ethylene-rich stream over diphenyl sulfide-modified Pd/SiO_2. (**A**) Acetylene/hydrogen conversions and product selectivities as a function of 1/WHSV (reaction conditions: 373 K; 0.9 kPa H_2, 0.6 kPa acetylene, 49.3 kPa ethylene, 0.6 kPa propane, 48.6 kPa N_2; WHSV = 0.031–0.63 $g_{acetylene}$ $g_{catalyst}^{-1}$ h^{-1}). (**B**) Long-term reaction data at the 1/WHSV of 4.83 h.

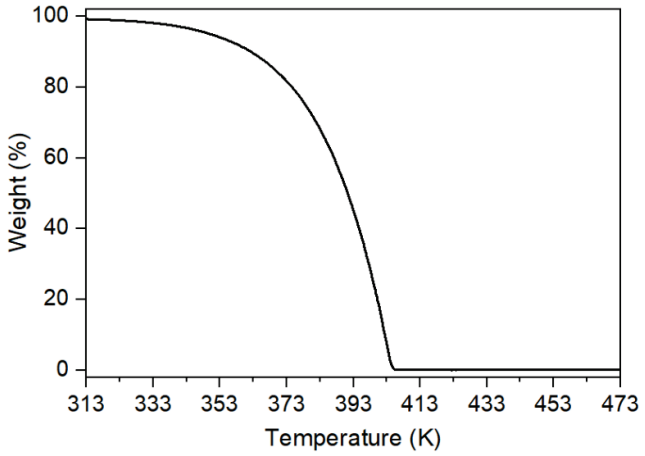

Fig. S13. Thermogravimetric analysis of diphenyl sulfide. Temperature was increased in a ramping rate of 2 K min^{-1} under H_2 atmosphere.

Table S1. EXAFS fitting results of the catalysts.

sample (reaction time[a])	shell	CN[b]	R (Å) [c]	σ^2 (Å^2) [d]	ΔE_0 (eV)	R-factor
Pd/PPS (0 h)	Pd–Pd	9.24 (±0.41)	2.758 (± 0.004)	0.0087 (±0.0005)	-5.19 (± 0.43)	0.0076
Pd/PPS (200 h)	Pd–Pd	9.28 (±0.43)	2.756 (± 0.004)	0.0085 (±0.0005)	-5.49 (± 0.44)	0.0142
Pd/SiO_2 (0 h)	Pd–Pd	9.41 (±0.41)	2.751 (± 0.004)	0.0082 (±0.0003)	-7.5 (± 0.44)	0.0151
Pd/SiO_2 (200 h)	Pd–Pd	9.56 (±0.37)	2.754 (± 0.004)	0.0080 (±0.0004)	-6.31 (± 0.37)	0.0098
Pd/*c*-PPS (0 h)	Pd–Pd	9.30 (±0.52)	2.770 (±0.005)	0.0096 (±0.0004)	-7.78 (± 0.55)	0.0169
Pd/*c*-PPS (200 h)	Pd–Pd	9.32 (±0.39)	2.758 (±0.003)	0.0083 (±0.0002)	-7.75 (± 0.41)	0.0096

[a]Acetylene hydrogenation reaction time in ethylene-rich stream for each catalyst. [b]Coordination number. [c]Interatomic distance. [d]Debye-Waller factor (σ).

REFERENCES AND NOTES

1. C. N. Satterfield, *Heterogeneous Catalysis in Industrial Practice* (McGraw-Hill, 1991).
2. T. W. van Deelen, C. Hernández Mejía, K. P. de Jong, Control of metal-support interactions in heterogeneous catalysts to enhance activity and selectivity. *Nat. Catal.* **2**, 955–970 (2019).
3. Y. Zhang, S. N. Riduan, Functional porous organic polymers for heterogeneous catalysis. *Chem. Soc. Rev.* **41**, 2083–2094 (2012).
4. P. Kaur, J. T. Hupp, S. T. Nguyen, Porous organic polymers in catalysis: Opportunities and challenges. *ACS Catal.* **1**, 819–835 (2011).
5. A. R. Riscoe, C. J. Wrasman, A. A. Herzing, A. S. Hoffman, A. Menon, A. Boubnov, M. Vargas, S. R. Bare, M. Cargnello, Transition state and product diffusion control by polymer–nanocrystal hybrid catalysts. *Nat. Catal.* **2**, 852–863 (2019).
6. S. Yun, S. Lee, S. Yook, H. A. Patel, C. T. Yavuz, M. Choi, Cross-linked "poisonous" polymer: Thermochemically stable catalyst support for tuning chemoselectivity. *ACS Catal.* **6**, 2435–2442 (2016).
7. A. S. Rahate, K. R. Nemade, S. A. Waghuley, Polyphenylene sulfide (PPS): State of the art and applications. *Rev. Chem. Eng.* **29**, 471–489 (2013).
8. Á. Molnár, A. Sárkány, M. Varga, Hydrogenation of carbon–carbon multiple bonds: Chemo-, regio- and stereo-selectivity. *J. Mol. Catal. A Chem.* **173**, 185–221 (2001).
9. A. Borodziński, G. C. Bond, Selective hydrogenation of ethyne in ethene-rich streams on palladium catalysts. Part 1. Effect of changes to the catalyst during reaction. *Catal. Rev.* **48**, 91–144 (2006).
10. A. J. McCue, J. A. Anderson, Recent advances in selective acetylene hydrogenation using palladium containing catalysts. *Front. Chem. Sci. Eng.* **9**, 142–153 (2015).
11. F. Huang, Y. Deng, Y. Chen, X. Cai, M. Peng, Z. Jia, P. Ren, D. Xiao, X. Wen, N. Wang, H. Liu, D. Ma, Atomically dispersed Pd on nanodiamond/graphene hybrid for selective hydrogenation of acetylene. *J. Am. Chem. Soc.* **140**, 13142–13146 (2018).
12. F. Huang, Y. Deng, Y. Chen, X. Cai, M. Peng, Z. Jia, J. Xie, D. Xiao, X. Wen, N. Wang, Z. Jiang, H. Liu, D. Ma, Anchoring Cu_1 species over nanodiamond-graphene for semi-hydrogenation of acetylene. *Nat. Commun.* **10**, 4431 (2019).

13. V. Mazumder, S. Sun, Oleylamine-mediated synthesis of Pd nanoparticles for catalytic formic acid oxidation. *J. Am. Chem. Soc.* **131**, 4588–4589 (2009).
14. M. Choi, W. Heo, F. Kleitz, R. Ryoo, Facile synthesis of high quality mesoporous SBA-15 with enhanced control of the porous network connectivity and wall thickness. *Chem. Commun.* 1340–1341 (2003).
15. M. Choi, Z. Wu, E. Iglesia, Mercaptosilane-assisted synthesis of metal clusters within zeolites and catalytic consequences of encapsulation. *J. Am. Chem. Soc.* **132**, 9129–9137 (2010).
16. S. M. Foiles, M. I. Baskes, M. S. Daw, Embedded-atom-method functions for the fcc metals Cu, Ag, Au, Ni, Pd, Pt, and their alloys. *Phys. Rev. B* **33**, 7983–7991 (1986).
17. G. Vilé, D. Albani, N. Almora-Barrios, N. López, J. Péréz-Ramírez, Advances in the design of nanostructured catalysts for selective hydrogenation. *ChemCatChem* **8**, 21–33 (2016).
18. I. Y. Ahn, J. H. Lee, S. K. Kim, S. H. Moon, Three-stage deactivation of Pd/SiO_2 and Pd-Ag/SiO_2 catalysts during the selective hydrogenation of acetylene. *Appl. Catal. A* **360**, 38–42 (2009).
19. S. J. Tauster, Strong metal-support interactions. *Acc. Chem. Res.* **20**, 389–394 (1987).
20. S. J. Tauster, S. C. Fung, R. T. K. Baker, J. A. Horsley, Strong interactions in supported-metal catalysts. *Science* **211**, 1121–1125 (1981).
21. J. C. Matsubu, S. Zhang, L. DeRita, N. S. Marinkovic, J. G. Chen, G. W. Graham, X. Pan, P. Christopher, Adsorbate-mediated strong metal-support interactions in oxide-supported Rh catalysts. *Nat. Chem.* **9**, 120–127 (2017).
22. D. W. Goodman, “Catalytically active Au on titania”: Yet another example of a strong metal support interaction (SMSI)? *Catal. Lett.* **99**, 1–4 (2005).
23. M. S. Chen, D. W. Goodman, The structure of catalytically active gold on titania. *Science* **306**, 252–255 (2004).
24. L. R. Baker, G. Kennedy, M. Van Spronsen, A. Hervier, X. Cai, S. Chen, L.-W. Wang, G. A. Somorjai, Furfuraldehyde hydrogenation on titanium oxide-supported platinum nanoparticles studied by sum frequency generation vibrational spectroscopy: Acid-base catalysis explains the molecular origin of strong metal–Support interactions. *J. Am. Chem. Soc.* **134**, 14208–14216 (2012).

25. H. Tang, Y. Su, B. Zhang, A. F. Lee, M. A. Isaacs, K. Wilson, L. Li, Y. Ren, J. Huang, M. Haruta, B. Qiao, X. Liu, C. Jin, D. Su, J. Wang, T. Zhang, Classical strong metal-support interactions between gold nanoparticles and titanium dioxide. *Sci. Adv.* **3**, e1700231 (2017).
26. C. H. Mejía, T. W. van Deelen, K. P. de Jong, Activity enhancement of cobalt catalysts by tuning metal-support interactions. *Nat. Commun.* **9**, 4459 (2018).
27. S. Nosé, A unified formulation of the constant temperature molecular dynamics methods. *J. Chem. Phys.* **81**, 511–519 (1984).
28. W. G. Hoover, Canonical dynamics: Equilibrium phase-space distributions. *Phys. Rev. A* **31**, 1695–1697 (1985).
29. S. Plimpton, Fast parallel algorithms for short-range molecular dynamics. *J. Comput. Phys.* **117**, 1–19 (1995).
30. S. L. Mayo, B. D. Olafson, W. A. Goddard, DREIDING: A generic force field for molecular simulations. *J. Phys. Chem.* **94**, 8897–8909 (1990).
31. A. K. Rappe, W. A. Goddard III, Charge equilibration for molecular dynamics simulations. *J. Phys. Chem.* **95**, 3358–3363 (1991).
32. R. K. Goyal, K. R. Kambale, S. S. Nene, B. S. Selukar, S. Arbuj, U. P. Mulik, Fabrication, thermal and electrical properties of polyphenylene sulphide/copper composites. *Mater. Chem. Phys.* **128**, 114–120 (2011).
33. A. K. Rappe, C. J. Casewit, K. S. Colwell, W. A. Goddard III, W. M. Skiff, UFF, a full periodic table force field for molecular mechanics and molecular dynamics simulations. *J. Am. Chem. Soc.* **114**, 10024–10035 (1992).
34. G. Kresse, J. Furthmüller, Efficiency of ab-initio total energy calculations for metals and semiconductors using a plane-wave basis set. *Comput. Mater. Sci.* **6**, 15–50 (1996).
35. G. Kresse, D. Joubert, From ultrasoft pseudopotentials to the projector augmented-wave method. *Phys. Rev. B* **59**, 1758–1775 (1999).
36. J. P. Perdew, K. Burke, M. Ernzerhof, Generalized gradient approximation made simple. *Phys. Rev. Lett.* **77**, 3865–3868 (1996).
37. S. Grimme, J. Antony, S. Ehrlich, H. Krieg, A consistent and accurate *ab initio* parametrization of density functional dispersion correction (DFT-D) for the 94 elements H-Pu. *J. Chem. Phys.* **132**, 154104 (2010).

38. B. J. Tabor, E. P. Magré, J. Boon, The crystal structure of poly-*p*-phenylene sulphide. *Eur. Polym. J.* **7**, 1127–1133 (1971).
39. C. H. Rycroft, G. S. Grest, J. W. Landry, M. Z. Bazant, Analysis of granular flow in a pebble-bed nuclear reactor. *Phys. Rev. E* **74**, 021306 (2006).